A new time-space accounting scheme to predict stream water residence time and hydrograph source components at the watershed scale

Takahiro Sayama[1,2] and Jeffrey J. McDonnell[1]

Received 27 October 2008; revised 19 April 2009; accepted 13 May 2009; published 1 July 2009.

[1] Hydrograph source components and stream water residence time are fundamental behavioral descriptors of watersheds but, as yet, are poorly represented in most rainfall-runoff models. We present a new time-space accounting scheme (T-SAS) to simulate the pre-event and event water fractions, mean residence time, and spatial source of streamflow at the watershed scale. We use a physically based hydrologic model together with field data from the well-studied Maimai M8 watershed and HJ Andrews WS10 watershed to explore how catchment properties, particularly soil depth, controls the age and source of streamflow. Our model simulates unsaturated, saturated subsurface, and surface rainfall-runoff processes. We first demonstrate the ability of the model to capture hydrograph dynamics and compare the model flow component and age simulations against measured values at the two sites. We show that the T-SAS approach can capture flow and transport dynamics for the right dominant process reasons. We then conduct a series of virtual experiments by switching soil depths between the two watersheds to understand how soil depth and its distribution control water age and source. Results suggest that thicker soils increase mean residence time and damp its temporal dynamics in response to rainfall inputs. Soil depth influenced the geographic source of streamflow, whereas pre-event water sources became more concentrated to near stream zones as soil depth increased. Our T-SAS approach provides a learning tool for linking the dynamics of residence time and time-space sources of flow at the watershed scale and may be a useful framework for other distributed rainfall-runoff models.

Citation: Sayama, T., and J. J. McDonnell (2009), A new time-space accounting scheme to predict stream water residence time and hydrograph source components at the watershed scale, *Water Resour. Res.*, *45*, W07401, doi:10.1029/2008WR007549.

1. Introduction

[2] "Accurate prediction of the headwater hydrograph implies adequate modeling of sources, flowpaths and residence time of water and solutes." *Hewlett and Troendle* [1975, p. 21] made this statement over thirty years ago. At that time, they were noting that while many different models could simulate an accurate hydrograph from the hillslope into the first-order stream, what makes such a prediction meaningful is getting the hydrograph right for the right reasons. Sadly, even with today's modern computing tools, new streamflow process insights [*McDonnell et al.*, 2007] and increasing demand for models that capture dynamics for the right reasons [*Beven*, 2002; *Kirchner*, 2006], we have few models that have been evaluated with field data to ensure adequate modeling of sources, flowpaths and residence time of water and solutes.

[3] One impediment is that we are not yet able to deconvolve a storm hydrograph into the rain parcels that express themselves at varying times in streamflow (Figure 1a) nor are we able to apportion within a hydrograph the geographic sources of flow through the event (Figure 1b). This is a fundamental theoretical challenge for hydrological modeling and a pressing applied need for nonpoint source pollution quantification, landuse change determination on flow and how climate impacts are expressed at the watershed outlet.

[4] Some recent runoff models have begun to incorporate flow source and age components into model development [*Uhlenbrook and Leibundgut*, 2002; *Seibert and McDonnell*, 2002; *Dunn et al.*, 2007] and evaluation [*Vache and McDonnell*, 2006; *Fenicia et al.*, 2008]. However, all of these models simply track tracers and do not record the history of solute progression in space through the watershed, thus thwarting analysis and interpretation of stream water source apportionment and its link to residence time. For example, we estimate mean residence time based on a simulated breakthrough curve from instantaneous tracer injection within a model. As a result, we can only predict a static residence time distribution for the entire simulation period and have no ability to quantify the dynamics of residence time distributions with flow conditions and rainfall regimes. Similarly, we do not know the relationship between the source components of flow (in time and space) and the residence time because no model approaches (that

[1]Department of Forest Engineering, Resources and Management, Oregon State University, Corvallis, Oregon, USA.
[2]Disaster Prevention Research Institute, Kyoto University, Gokasho Uji, Kyoto, Japan.

0043-1397/09/2008WR007549$09.00

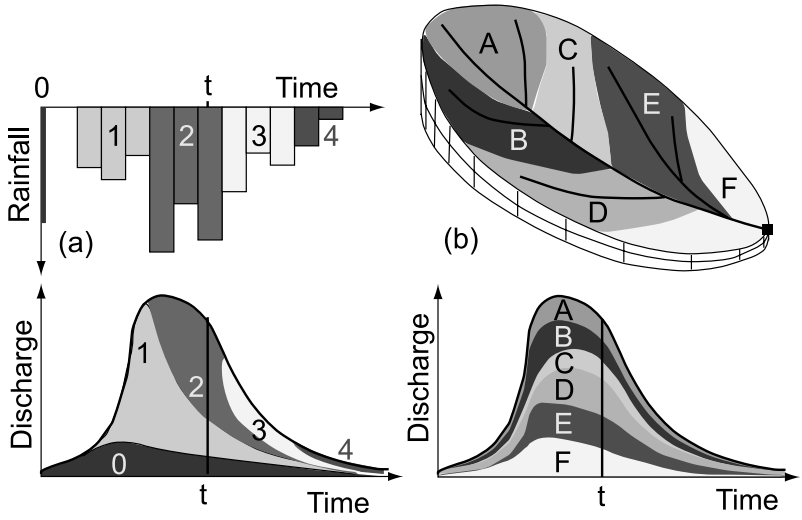

Figure 1. Schematic diagram of our approach; namely the separation of the temporal and spatial hydrograph components. (a) Individual rainfall hyetograph segments are propagated through the storm hydrograph. (b) The geographic source apportionment of flow.

we are aware of) have developed or included such an accounting scheme to deconvolve a simulated hydrograph as illustrated by Figure 1.

[5] Such a model and approach could be evaluated at watersheds with high quality time source information (typically gained from two-component isotope hydrograph separation studies), geographic source information (typically gained from geochemical end-member mixing analysis) and mean residence time information of soil water and stream water (typically gained from time series of stable isotope information). A model set up and tested in such a way could be enormously helpful in addressing some of the outstanding questions in catchment science: How does residence time vary with flow regime? How are flow sources and residence time related? How do catchment characteristics control the time and geographic sources of streamflow? Perhaps most importantly, such an approach could lead to the development of routine evaluative measures for models that can then be tested (and rejected) with field data and thus ensuring adequate modeling of sources, flowpaths and residence time of water and solutes, as Hewlett and Hibbert called for so long ago.

[6] Here we develop a new matrix accounting scheme to enable time and source separation of the hydrograph as a pathway to new understanding of the controls on hydrograph sources and residence time of water at the watershed scale. We use two well studied experimental watersheds (the Maimai watershed in New Zealand and the HJ Andrews Experimental watershed in Oregon USA) as proof of concept for the approach. We then perform a series of virtual experiments [*Weiler and McDonnell*, 2004] using these systems as shells for combinations of rainfall regime and soil depth distributions to further our understanding on the physical controls on water flow, source and residence time dynamics at the watershed scale. The specific questions we address in this paper are:

[7] 1. Can a time-space accounting scheme for hydrologic models be developed to link time and geographic sources of flow in a watershed?

[8] 2. Can a hydrologic model incorporating a time-space accounting scheme express the observed findings of pre-event and event water fractions and residence time?

[9] 3. How does residence time vary with time throughout the hydrologic year?

[10] 4. What is the interaction between sources and age of flow at the watershed scale?

[11] 5. What is the dominant catchment property controlling the interaction of sources and age of flow in the stream?

2. Methods

2.1. Hydrologic Model

[12] We use the distributed rainfall-runoff model OHDIS-KWMSS (OHymos-based DIStributed model, with Kinematic Wave Method for Surface and Subsurface runoff [*Tachikawa et al.*, 2004]) in our analysis. It is important to point out that the new accounting procedure (described below) could be used with any number of distributed hydrologic models now in use. We apply it to OHDIS-KWMSS because this is a model we have used previously [*Sayama et al.*, 2006; *Tachikawa et al.*, 2006] and have familiarity with. OHDIS-KWMSS simulates surface and subsurface flow. Among the distributed models reviewed by *Kampf and Burges* [2007] OHDIS-KWMSS is perhaps most similar to TOPKAPI [*Ciarapica and Todini*, 2002] where, like TOPKAPI, it uses a kinematic approximation for unsaturated lateral flow. OHDIS-KWMSS accounts for flow in capillary and noncapillary pore space with a single set of storage-discharge equation; it is thus able to capture dynamics in steep humid catchments such as rapid subsurface stormflow in a layer of limited thickness and high hydraulic conductivity due to the preferential flow paths and macroporosity.

[13] Like many other distributed models (e.g., DHSVM as reported by *Wigmosta et al.* [1994], Hill-VI as reported by *Weiler and McDonnell* [2004], etc.), catchment topography in OHDIS-KWMSS is represented with a set of

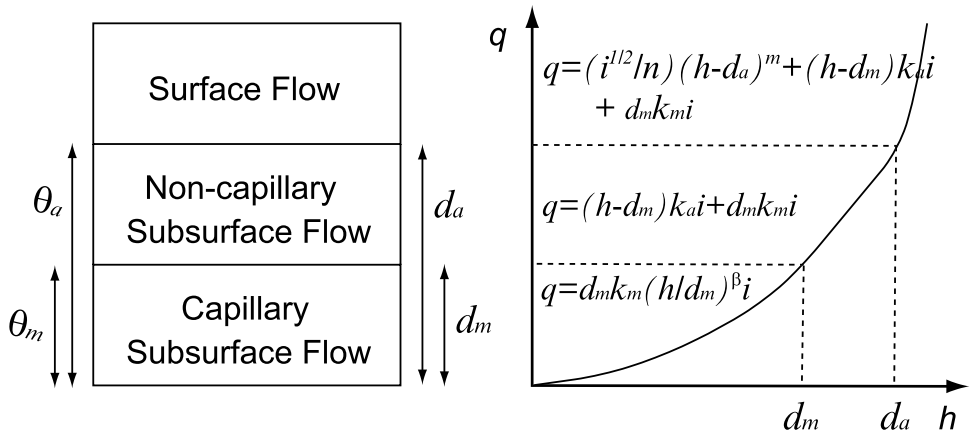

Figure 2. Graphical representation of the OHDIS-KWMSS model illustrating how flow (q) is calculated based on water table height (h) in each pixel.

pixels, which are covered by soil with capillary pore space and noncapillary pore space on a impermeable bedrock (Figure 2).

[14] When the volumetric water content θ is smaller than the maximum volumetric water content in the capillary pore θ_m, the water flows in the capillary pore as unsaturated subsurface flow, which is modeled by the Darcy equation with a variable hydraulic conductivity k. By using the power form of k ($= k_m S_e^{\beta}$ [*Leibenzon*, 1947]) and by assuming that the hydraulic gradient is equal to the slope of ground surface, the average velocity in the downslope direction in the capillary pore v_m is estimated as:

$$\begin{aligned} v_m &= -k\left(\frac{\partial H}{\partial x}\right) \\ &= k_m S_e^{\beta}\left(i - \frac{\partial \varphi}{\partial x}\right) \\ &= k_m \left(\frac{\theta}{\theta_m}\right)^{\beta}\left(i - \frac{\partial \varphi}{\partial x}\right) \\ &\cong k_m \left(\frac{\theta}{\theta_m}\right)^{\beta} i \\ &= k_m \left(\frac{h}{d_m}\right)^{\beta} i \end{aligned} \tag{1}$$

where H is a hydraulic head; φ is a pressure head; x is a distance in lateral direction; S_e ($= \theta/\theta_m$) is a degree of saturation; i is a slope; k_m is a saturated hydraulic conductivity in capillary pore; β is an exponent parameter; h is an equivalent water stage ($h = D\theta$), where D is a soil depth; d_m is an equivalent water stage to the maximum water content in the capillary pore ($d_m = D\theta_m$). For unsaturated conditions ($0 \le \theta < \theta_m$), or ($0 \le h < d_m$), lateral discharge from a pixel per unit width q is

$$q = d_m k_m \left(\frac{h}{d_m}\right)^{\beta} i. \tag{2}$$

[15] When the volumetric water content θ exceeds the maximum water content in the capillary pore θ_m, the water flows in the noncapillary and capillary pore as saturated subsurface flow, which is modeled by the Darcy equation with saturated hydraulic conductivities. The average velocity in the noncapillary pore v_a is estimated by

$$v_a = k_a i \tag{3}$$

where k_a is saturated hydraulic conductivity in noncapillary pore. The total discharge per unit with q is estimated by adding subsurface flow in noncapillary pore and capillary pore

$$q = (h - d_m)k_a i + d_m k_m i. \tag{4}$$

[16] To assure the continuity of the discharge change when $h = d_m$, the derivations of $q(h)$ calculated from equations (2) and (4) are set to be equal when $h = d_m$. Then we obtain the following relationship:

$$\beta k_m = k_a. \tag{5}$$

It is reasonable that $k_a > k_m$ when $\beta > 1$. By adopting this relationship, we can reduce one model parameter k_m.

[17] When the volumetric water content exceeds the effective porosity θ_a, saturation excess overland flow occurs, which is modeled by the Manning equation. The average velocity of overland flow is estimated with Manning's roughness coefficient n [*Takasao and Shiiba*, 1988]:

$$v_s = k_a i + \frac{\sqrt{i}}{n}(h - d_a)^{m-1}. \tag{6}$$

[18] The total discharge q is estimated by adding overland flow and subsurface flow in noncapillary pore and capillary pores

$$\begin{aligned} q &= (h - d_a)v_s + (d_a - d_m)v_a + d_m v_m \\ &= \frac{\sqrt{i}}{n}(h - d_a)^m + (h - d_m)k_a i + d_m k_m i. \end{aligned} \tag{7}$$

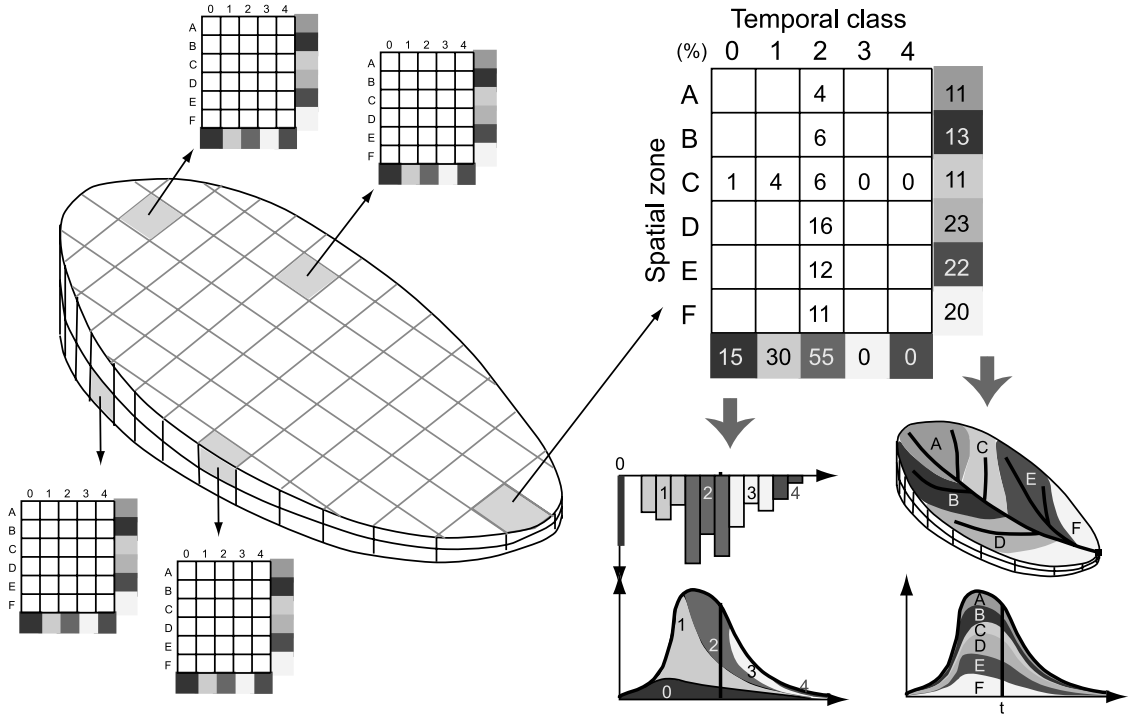

Figure 3. Schematic representation of the T-SAS approach. The T-SAS matrix shows how the ratio of water from different temporal classes and spatial zones are computed where the numbers inside the matrix are added vertically and horizontally (in the diagram) to compute the value(s) shown in the shaded part outside of the matrix. These shaded numbers correspond to the percentage of the shaded areas in the hydrograph. The T-SAS matrices are assigned to each pixel for each of the flow pathway (surface, capillary, and noncapillary flow) such that all the matrix values are updated in a downslope direction.

[19] Finally, the discharge-stage relationship illustrated in Figure 2, and the continuity equation, are used to simulate rainfall-runoff in each pixel

$$q = \begin{cases} d_m k_m \left(\dfrac{h}{d_m}\right)^{\beta} i, & (0 \le h \le d_m) \\ (h - d_m) k_a i + d_m k_m i, & (d_m < h \le d_a) \\ \dfrac{\sqrt{i}}{n}(h - d_a)^m + (h - d_m) k_a i + d_m k_m i & (d_a < h) \end{cases} \tag{8}$$

$$\frac{\partial h}{\partial t} + \frac{\partial q}{\partial x} = r(t) \tag{9}$$

where $r(t)$ is effective rainfall, which is equivalent to the difference between rainfall and evapotranspiration rates.

2.2. Time-Space Accounting Scheme (T-SAS)

[20] We solve the time-space accounting challenge illustrated in Figure 1 using a matrix-based time-space accounting scheme (T-SAS) that tracks the ratio of flow contributed by rainwater originating from certain temporal classes and spatial zones (Figure 3). For time source hydrograph separation, we can divide rainfall into separate temporal classes (in this example we use five temporal classes from 0 to 4 depending on the time of the rainfall). The number of classes can be adjusted based on the number of discrete separate hydrograph components one wants to simulate. The 0 class represents rainwater prior to the beginning of the simulation (pre-event water), while the classes 1 to 4 represent rainwater (event water) in the different periods comprising the rainfall hyetograph. The colors in the hyetograph correspond to the colors in the hydrograph in Figure 1a, indicating when rainwater in the each period exist the outlet of the catchment. T-SAS performs the spatial source separation of streamflow following the concept outlined in Figure 1b. The catchment is divided into the six zones from A to F, and the separated hydrograph in Figure 1b illustrates when rainwater in the different zones exists the catchment outlet. The key feature is the combination of, and accounting for, the spatiotemporal sources of streamflow simultaneously.

[21] Provided the number of spatial zones and temporal classes are defined as S and T respectively, the dimension of the T-SAS matrix $\boldsymbol{R}_i(t)$ is $(S \times T)$. For example, the matrix in Figure 3 represents the constituents of water flowing at the catchment outlet. It shows that 6% of the discharge is sourced from rainwater during temporal class 2 and spatial zone C. Adding all the values in rows for each column, we can obtain the ratio of the flow originating from each temporal class. Consequently, the hydrograph at time t can be separated based on the temporal sources of streamflow as shown in Figure 1a. In this example, rainwater during temporal class 0, or pre-event water, comprises 15% of the discharge at time t, and rainwater during temporal class 1 equals 30%. Adding all the values from side to side for each row, we can separate the hydrograph at time t based on the spatial sources of streamflow. In this example rainwater in the spatial zones A and B contribute 11% and 13% of the discharge, respectively.

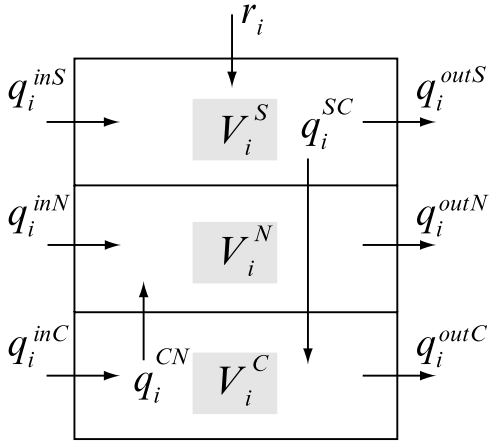

Figure 4. Flow components and volume that have to be calculated before T-SAS tracking for each flowpath in each pixel.

[22] The temporal source and the spatial source of water differ depending on the location. In addition, even at the same location the temporal and spatial sources must be different depending on the flowpaths. Therefore our new method assigns different T-SAS matrix to each flow pathway at each pixel in a distributed rainfall-runoff model (Figure 3, left). The matrices are then updated from upper areas to lower areas by the method explained in the next section.

2.3. Tracking the T-SAS Matrix for Each Flow Pathway at Each Pixel

[23] In order to update the T-SAS matrix, we first calculate the discharge q_i and water stage h_i at each pixel with the rainfall-runoff model. We then calculate all the discharge and volume components represented with the arrows in Figure 4 where q_i^{inS}, q_i^{inN} and q_i^{inC} denote inflows to surface, noncapillary pore space and capillary pore space at each pixel i; q_i^{SC} denotes discharge from surface to noncapillary pore space and q_i^{CN} denotes discharge from capillary pore space to noncapillary pore space. Note that q_i^{SC} and q_i^{CN} become negative if the flow directions are opposite. All of these flow components are calculated at each time step with mass balance equations based on the water stage at each pixel.

[24] Based on the calculated discharge components for each pixel, we update the T-SAS matrix values by the following equations for surface flow $\boldsymbol{R}_i^S$, subsurface flow in noncapillary pore space $\boldsymbol{R}_i^N$ and in capillary pore space $\boldsymbol{R}_i^C$ $\boldsymbol{R}_i^C$ in each pixel:

$$\frac{d\left(V_i^S \boldsymbol{R}_i^S\right)}{dt} = \sum_{j \in U_i} q_j^{outS} \boldsymbol{R}_j^S - q_i^{outS} \boldsymbol{R}_i^S - q_i^{SC} \boldsymbol{R}_i^{SC} + r_i A_i \boldsymbol{R}_i^{rain} \quad (10)$$

$$\frac{d\left(V_i^N \boldsymbol{R}_i^N\right)}{dt} = \sum_{j \in U_i} q_j^{outN} \boldsymbol{R}_j^N - q_i^{outN} \boldsymbol{R}_i^N + q_i^{CN} \boldsymbol{R}_i^{CN} \quad (11)$$

$$\frac{d\left(V_i^C \boldsymbol{R}_i^C\right)}{dt} = \sum_{j \in U_i} q_j^{outC} \boldsymbol{R}_j^C - q_i^{outC} \boldsymbol{R}_i^C + q_i^{SC} \boldsymbol{R}_i^{SC} - q_i^{CN} \boldsymbol{R}_i^{CN} \quad (12)$$

$$\boldsymbol{R}_i^{SC} = \begin{cases} \boldsymbol{R}_i^S & \left(q_i^{SC} \geq 0\right) \\ \boldsymbol{R}_i^C & \left(q_i^{SC} < 0\right) \end{cases} \quad (13)$$

$$\boldsymbol{R}_i^{CN} = \begin{cases} \boldsymbol{R}_i^C & \left(q_i^{CN} \geq 0\right) \\ \boldsymbol{R}_i^N & \left(q_i^{CN} < 0\right) \end{cases} \quad (14)$$

where V_i^S, V_i^N and V_i^C are the water volumes stored at each flow pathway; A_i is projected area of the pixel; $\boldsymbol{R}_j^S$, $\boldsymbol{R}_j^N$ and $\boldsymbol{R}_j^C$ are the T-SAS matrices of the adjacent upslope pixel j. The calculation of the matrices is done from the upslope area downward so that $\boldsymbol{R}_j^S$, $\boldsymbol{R}_j^N$ and $\boldsymbol{R}_j^C$ become known variables before calculating $\boldsymbol{R}_i^S$, $\boldsymbol{R}_i^N$ and $\boldsymbol{R}_i^C$. $\boldsymbol{R}_i^{Rain}$ is the T-SAS matrix of rainwater at i. It has a value of 1 only at the element of (t, i) in the matrix. The term $r_i A_i \boldsymbol{R}_i^{rain}$ is added to the right side of equation (10) based on the assumption that rainwater is mixed with surface flow. If no surface flow ($h < d_a$) occurs at the pixel i, the $r_i A_i \boldsymbol{R}_i^{rain}$ term is added to the right side of equation (12) by assuming that the rainwater directly reaches to the subsurface flow via capillary pores.

[25] The T-SAS matrix tracking equations are obtained through mass balance equations. It simulates explicitly advective transport of water among the different flowpaths (surface flow and subsurface flow in noncapillary space and in capillary space) at different pixels. Dispersion is not explicitly modeled in order to keep the method simple. Nevertheless, the numerical dispersion effect is still included as per *Vache and McDonnell* [2006]. The T-SAS approach assumes also the instantaneous and complete mixing within an associated water volume for each flowpath at each pixel. (Note that the assumptions here are different from the homogeneous and complete mixing at the entire catchment assumed in the ordinary two component mixing approach because T-SAS still tracks the temporally and spatially heterogeneous matrix information.) It does not parameterize the effect of immobile water and mixing rate within a pixel and a flowpath as some recent studies have proposed [*Page et al.*, 2007; *Iorgulescu et al.*, 2007]. Instead of introducing additional parameters to simulate tracers, we trace the time and space information simply by following the modeled runoff processes with parameters used for the rainfall-runoff model. If an applied model cannot reproduce the observed residence time or the expected spatial source of water, one can reconsider the model structure for example, by simulating additional flow pathways. The main difference between T-SAS approach and the standard tracer simulation method is that unlike the standard method, which tracks a single type of conservative tracer inside a model [*Uhlenbrook and Leibundgut*, 2002; *Uhlenbrook et al.*, 2004; *Wissmeier and Uhlenbrook*, 2007; *McGuire et al.*, 2007; *Dunn et al.*, 2007; *Son and Sivapalan*, 2007] is that our approach simultaneously tracks multiple virtual tracers by updating T-SAS matrix. Each of the elements of T-SAS matrix represents rainwater falling in a pixel and a certain time increment. Consequently, it can calculate time and space sources of soil water and surface water for each pixel.

[26] Our ultimate goal is to separate a stream hydrograph based on time and space sources. Therefore after calculating all the matrix values for all pixels, we calculate the T-SAS

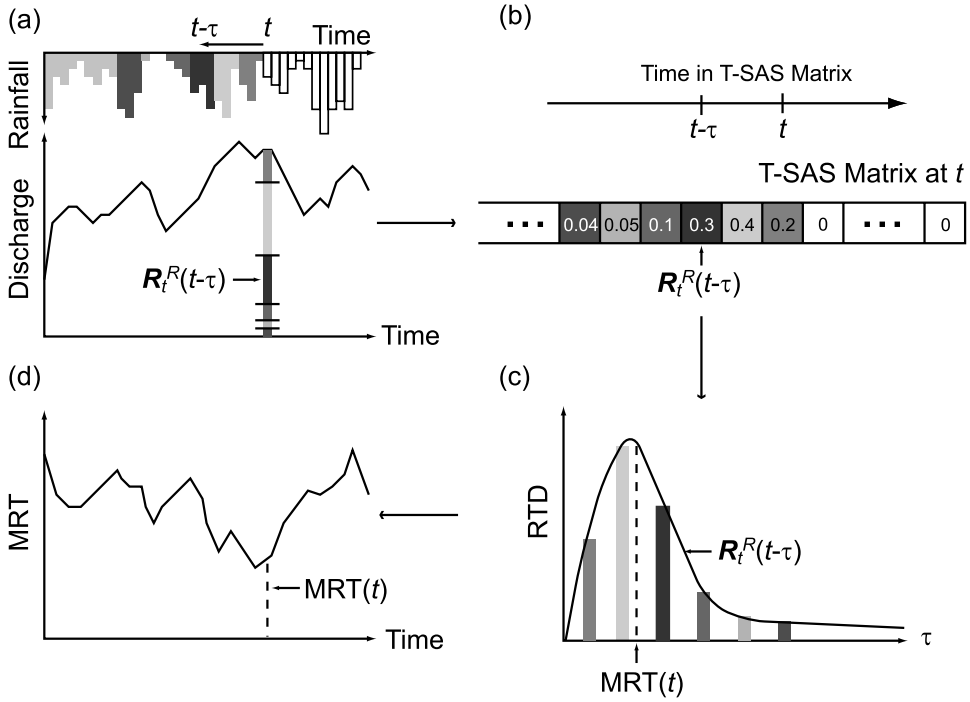

Figure 5. Calculation of mean residence time (MRT) with the T-SAS method. (a) Uses the temporal hydrograph separation developed in Figure 3 to separate the hydrograph into daily values, where $\boldsymbol{R}$ is the percentage of flow from a given precipitation time input at $(t - \tau)$. (b) The numerical values for the temporal components of flow at time t. (c) Residence time distribution (RTD) for time t calculated using the T-SAS matrix values. (d) Finally, the MRT for the 1-year time series is illustrated schematically showing how the discrete daily MRT calculated from Figure 5c corresponds to other values through the year.

matrix in the stream by summing up the matrix values adjacent to the stream with the following equation:

$$\boldsymbol{R}^R = \frac{\sum_{i \in C} \left(q_i^{outS} \boldsymbol{R}_i^S + q_i^{outN} \boldsymbol{R}_i^N + q_i^{outC} \boldsymbol{R}_i^C \right)}{\sum_{i \in C} \left(q_i^{outS} + q_i^{outN} + q_i^{outC} \right)} \tag{15}$$

where $\boldsymbol{R}_i^R$ is the T-SAS matrix of stream water, and $i \in C$ indicates all the pixels that flow directly into the stream. Once the T-SAS matrix is known in the stream, the separation of the hydrograph by temporal sources and spatial sources is easily completed.

2.4. Mean Residence Time Calculation Based on the T-SAS Matrix

[27] Mean residence time (MRT) of stream water (sometimes referred to as transit time [*McGuire and McDonnell*, 2006]) has been recognized as a useful index to represent the hydrologic processes and flowpaths at the watershed scale. We define residence time as the time elapsed since the water molecule entered the catchment as recharge to when it exits at the catchment outlet. Since the stream water at anytime is the assemblage of water molecules through different flowpaths, the residence time of streamflow is described as a probability density function, which we call the Residence Time Distribution (RTD). Therefore the mean of RTD is the MRT [*McGuire and McDonnell*, 2006]. Here we explain how we calculate the RTD and MRT based on the T-SAS matrix. Figure 5a shows how we first simulate rainfall-runoff for a long term period and apply the T-SAS algorithm to separate the hydrograph based on the rainwater temporal classes. In the present case study, we separated the hydrograph into rainwater originating from different days. As a result, the calculated stream T-SAS matrix $\boldsymbol{R}_t^R$ (Figure 5b) indicates the ratio of the rainwater contribution from the first day to the day at time step t. Since the $\boldsymbol{R}_t^R$ is equivalent to the RTD for the time step t (Figure 5c), we can calculate the MRT with the following equation.

$$MRT(t) = \sum_{\tau=o}^{t} \tau \boldsymbol{R}_t^R(t - \tau) \tag{16}$$

Note the calculated value represents the MRT of streamflow at time step t. As we separate the hydrograph for each time step, the RTD and MRT can be obtained for all the time steps; consequently the temporal variation of MRT can be estimated as shown in Figure 5d.

3. Study Sites Used for Model Development and Testing

[28] We show proof of concept of our model and T-SAS methodology using two very well studied watersheds where extensive source information and residence time estimates have been made: the Maimai (M8) in New Zealand and the HJ Andrews (WS10) in Oregon USA. The two watersheds are very similar in terms of their wet climate regime, high runoff ratios and steep forested slopes but differ in terms of

Table 1. Watershed Attributes for M8 and WS10 Based on Measured Values and Calculations From Field Studies at the Two Sites

	M8	Reference	WS10	Reference
Area (ha)	3.8	*McDonnell* [1990]	10.2	*Harr* [1977]
Annual rainfall (mm)	2600	*Rowe and Pearce* [1994]	2220	*McGuire et al.* [2007]
Runoff coefficient (%)	60	*Rowe and Pearce* [1994]	56	*McGuire et al.* [2007]
Average slope (°)	34	*McDonnell* [1990]	30	*McGuire et al.* [2005]
Mean soil depth (m)	0.7	*Mosley* [1979]	3.0	*Harr and Ranken* [1972]
Pre-event water ratio (%)	75–85	*Sklash et al.* [1986]	> 70	*McGuire* [2004]
Stream W. MRT	4 months	*Pearce et al.* [1986]	1.2 years	*McGuire et al.* [2005]

the timing of their rainfall regime and soil depth distributions. As such, these test catchments offer contrasts in the two main variables we later use to understand the physical controls on, and linkages between, flow, source and residence time.

3.1. Maimai M8 Watershed

[29] The Maimai M8 is a 3.8 ha watershed located on the West Coast of the South Island of New Zealand (42.1° S, 171.8° E). *McGlynn et al.* [2002] provided a review of hydrological research at Maimai and we base our brief summary on their description of the site. Mean annual precipitation averages 2600 mm. The summer months are the driest; average monthly rainfall from December to February is 165 mm per month and is between 190 and 270 mm per month for the rest of the year. Typically, there are only about 2 snow days per year. The catchment is highly responsive to storm rainfall, and on average 60 % of annual precipitation becomes runoff [*Rowe and Pearce*, 1994]. Slopes are short (<300 m), steep (average 34°), and have local relief ranging from 100–150 m. A moderately weathered, early Pleistocene conglomerate, known as the Old Man Gravels, underlies the Maimai catchment. The conglomerate is comprised of clasts of sandstone, granite, and schist in a tight clay-sand matrix and is nearly impermeable, with estimates of seepage losses to deep groundwater of only 100 mm y-1 [*Rowe and Pearce*, 1994]. Soils overlying the Old Man Gravels are classified as Blackball Hill soils. Silt loam textures predominate. Typical soil profiles are characterized by thick, well developed organic horizons (∼17 cm), thin, slightly stony, dark grayish brown A horizons, and moderately thick, very friable mineral layers of podsolized, stony, yellow-brown earth subsoils (∼60 cm). The vegetation is mixed evergreen beech forest (*Nothofagus* spp.), podocarpus, and broad-leafed hardwoods.

3.2. HJ Andrews WS10

[30] Watershed-10 (WS10) is a 10.2 ha watershed located at the H.J. Andrews Experimental Forest (HJA) in the west-central Cascade Mountains of Oregon, USA (44.2° N, 122.25° W). *McGuire et al.* [2005] has reviewed some of the recent hydrological research at the site and we base our brief summary here on their synopsis. Annual precipitation is 2220 mm (averaged from 1990 to 2002), about 80% of which falls between October and April during frequent, long duration, low to moderate intensity frontal storms. The climate is Mediterranean with strong contrasts between summer and winter precipitation amounts [*Greenland*, 1994]. The catchment experiences a gradual wet-up period from about October to December and thereafter maintains very high wetness until late spring. Snow accumulations are common, but seldom persist longer than 1–2 weeks and generally melt within 1–2 days. On average, 56% (28 to 76%) of the annual precipitation becomes runoff. Slopes are short (<200 m), steep (average 30%), and have local relief ranging from 60–130m. The catchment contains residual and colluvial clay loam soils derived from andesitic tuffs (30%) and coarse breccias (70%) comprising the Little Butte Formation formed as the result of ashfall and pyroclasitic flows from Oligocene-Early Miocene volcanic activity [*Swanson and James*, 1975]. Surface soils are well aggregated; however, lower depths (70–110 cm) exhibit more massive blocky structure with less aggregation than surface soils [*Harr*, 1977]. Beneath the weakly developed A and B horizons is partially weathered parent material (saprolite [*Harr and McCorison*, 1979; *Sollins and McCorison*, 1981]). The vegetation is dominated by a naturally regenerated second growth Douglas-fir (*Pseudotsuga menziesii*) stand resulting from a 1975 clear-cut harvest.

3.3. M8-WS10 Intercomparison of Flow Source and Residence Time

[31] Table 1 shows a summary of flow, source and residence time information for the two study watersheds. We use these as model targets for developing proof of concept for our T-SAS approach. With a model that hits these complementary data targets, we then progress to a series of virtual experiments aimed at exploring how soil depth and rainfall regime impact the interactions between source, flow and MRT and how these are expressed within the system spatially and recorded at the watershed outlet. Distributed soil depth values were used for WS10 from an available soils map at HJ Andrews Experimental Forest. These depths ranged from 1.5 m to 4.2 m with average soil depth of 3.0 m (Figure 6b). Mapped soil depth distributions for M8 were unavailable. Nevertheless, many field groups over the past decades have recorded soil depths at different discrete points within the watershed [*McKie*, 1978; *McDonnell*, 1990; *Woods and Rowe*, 1996] and distributed across subwatersheds within and adjacent to M8 [*Mosley*, 1979; *McDonnell*, 1997]. We used stream order to distribute and regionalize these point and partial soil depth distribution data across the watershed (Figure 6a) with an average soil depth set at 0.7 m following Mosley's extensive survey work in a 0.3 ha subcatchment of M8 [*Mosley*, 1979].

4. Results

4.1. Simulated Hydrographs

[32] We applied the OHDIS-KWMSS model to the two watersheds. The temporal resolution of the recorded rainfall

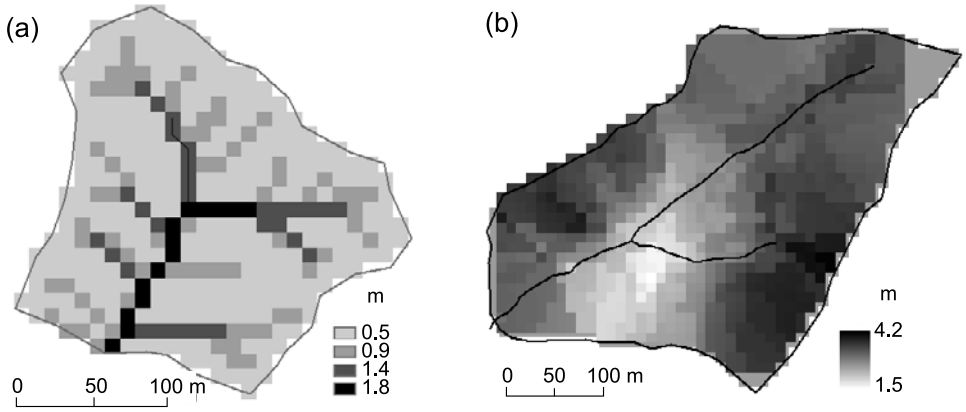

Figure 6. Soil depth maps for the (a) M8 and (b) WS10 watersheds. Note that the scale is different for the two watersheds, where soils are significantly deep in WS10.

input for M8 (WS10) was 20 (60) minutes. The ET was estimated with different methods at two sites. For M8 site, the daily totals were calculated based on five different standard methods, then transformed using a sine curve distribution between the hours of 6:00 and 18:00 [*Vache and McDonnell*, 2006]. For WS10 site, they were estimated by a temperature index method [*Hargreaves and Samani*, 1985], which was adopted by a previous HJ Andrews modeling study [*McGuire et al.*, 2007]. Model parameters were manually calibrated within the range of field observation [*McDonnell*, 1989; *McGuire*, 2004] to reproduce observed wet season hydrographs at each site: 2 September–31 December 1987 at M8 and 1 November 1999–29 February 2000 at WS10. We first tried the same parameter sets to simulate hydrographs at both sites, so that we could minimize the influence of parameters on the differences of T-SAS results between the two sites. Based on the simulations, we found that the same parameters could be used for n, k_a and β with 0.3 $m^{-1/3}s$, 0.005 m/s and 40, respectively. For the porosity parameters θ_a and θ_m, we used the different parameter values for the two sites: 0.55 and 0.35 (0.60 and 0.55) for M8 (WS10), which are consistent with the range of field observations. Figure 7 shows the observed and simulated discharge hydrographs at M8 (WS10). Nash Sutcliffe efficiencies were 0.91 (0.70). Even though the model does not reproduce the observed hydrographs perfectly during the low flow period at WS10, the model could generally simulate the different characteristics between the two watersheds; namely faster recessions at M8 and slower recessions at WS10.

4.2. Event Water/Pre-event Water Separations

[33] Figure 7 shows the T-SAS temporal hydrograph separation results for the period of simulated flow. The colors in the hydrographs correspond to the colors in the discrete hyetographs, except for the black portion which represents the stored water before the beginning of the simulations (1 October at M8 and 21 November at WS10). We defined this as our pre-event water (or old water). Note that the T-SAS hydrograph separation relaxes some of assumptions that are required for the traditional component mixing approach. For example, spatially homogeneity in the input and stored groundwater tracer signal, as well as their complete and instantaneous mixing within the entire catchment is assumed for the two component mixing approach. These assumptions can potentially cause significant errors in hydrograph separations [*Kendall et al.*, 2001]. Alternatively, T-SAS tracks imaginary time-space information of water with the form of T-SAS matrix, and

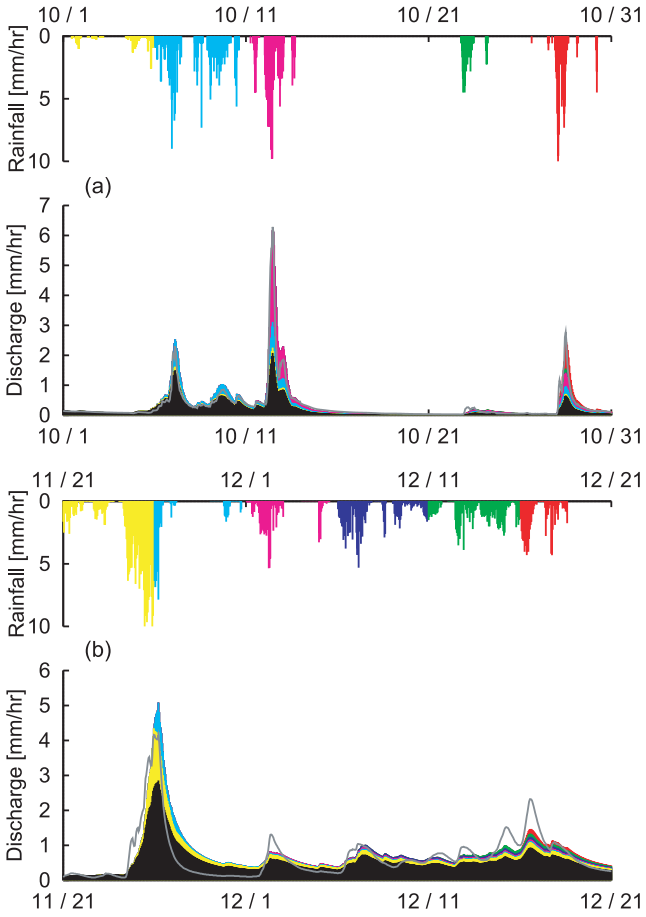

Figure 7. Temporal hydrograph separations at (a) M8 and (b) WS10. The black portions of the hydrographs represent pre-event water runoff, while the other colors in the hydrographs show the runoff that originated from the corresponding colors in the rainfall hyetographs. The solid lines show the observed hydrographs for each site.

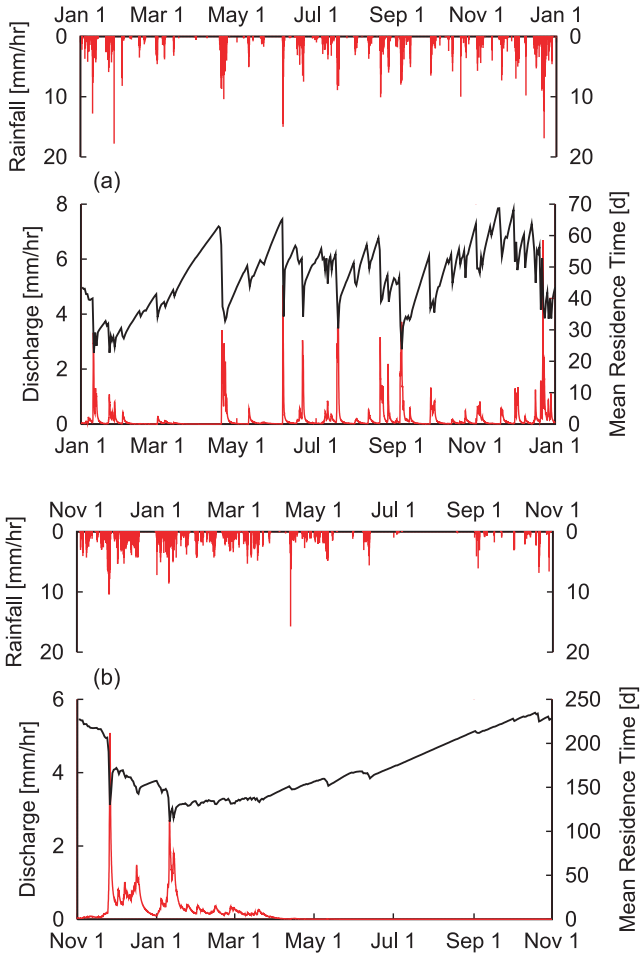

Figure 8. Time series of measured rainfall, modeled runoff using OHDIS, and calculated MRT using T-SAS for (a) M8 and (b) WS10. Note the very different temporal dynamics of MRT in the two watersheds.

therefore does not require any of the traditional homogeneity assumptions. As a result, T-SAS can perform the hydrograph deportation for catchment situations with heterogeneous inputs and storages where the conventional approach two-component mixing model would clearly fail. The percentage of pre-event water comprising the streamflow for the 30 day period was 53 % (71%) for M8 (WS10). This assumes that the pre-30-day-old water signature (shown in black in Figure 7) is the pre-event water that is propagated through the entire 30 day time series and used for the calculation of each of the individual hydrograph separations. If we were to define pre-event water as the rainwater falling to the watersheds prior to an individual storm, then the pre-event water ratio would be even higher (in most cases >70%). For example, during the last rainfall event at M8 that occurred 25 to 30 October (Figure 7a), the black shaded portion of the hydrograph represents the pre-event water in the system prior to the 30-day time series. It comprised 32% of the total runoff, whereas the pre-event water that includes all of the other colors (except the red which is the event water color for this event) comprised 41% of total flow during the event. Therefore if we performed the model calculation with pre-event water defined as the complete blend of colors prior to this particular storm, then the pre-event water amount would be the sum of 32 + 41% (73%). These results suggest that the simulated hydrographs using our simple kinematic wave model have high pre-event water fractions in the range of 60% to 75% for both catchments. These high pre-event water fractions are consistent with field data shown in Table 1.

4.3. MRT of Stream Water and Temporal Variation

[34] Field studies at M8 and WS10 have reported very different MRT values (Table 1). Reported MRT are about 4 months at M8 and 1.2 years at WS10. Our one of the scientific questions was whether or not the model can express the differences in MRT between the two watersheds. The simulation periods for the MRT were decided based on the availability of rainfall data for one year: from 1 January to 31 December in 1985 at M8 and from 1 November to 31 October in 1999 at WS10. Figure 8 shows the simulated hydrographs and MRT time series at M8 (WS10). Note that the MRT at the beginning of the simulation became equal to the MRT at the end of the simulation because the yearly rainfall series was assumed to be repeated in the previous years to calculate MRT.

[35] Estimated MRT at M8 (WS10) is 46 (173) days. The MRT at WS10 is about three times longer than that of M8. The model, with T-SAS accounting tool, can express adequately the difference of reported MRT between the two watersheds (about 3.5 times longer at HJA). Notwithstanding, the calculated MRT for both watersheds were about 40 % of the reported values. One of the reasons for the underestimates appears related to the within-period temporal variation of MRT. Figure 8 shows that the MRT during high flow may be shorter than the MRT during base flow (or what one might term the base flow MRT, the conditions under which most of water samples were collected for field-based MRT estimation reported in Table 1). Unlike the field-based base flow MRT, our model MRT values represent all flow conditions including base flow and high flow periods. If we compare only our estimated model-based MRT during base flow conditions, then our modeled values for both watersheds are within 60% of the measured data in Table 1.

[36] Figure 8 also shows the different characteristics of MRT time series in the two watersheds. MRT at M8 is more temporally dynamic and sensitive to rainfall inputs than is WS10, which shows a relatively stable MRT signal. Auto correlation for these two signals are 0.64 (0.93) at M8 (WS10). Notwithstanding these patterns, the seasonal variation of MRT is more significant at WS10 where the MRT standard deviation is 33 days (compared to 10 days at M8).

[37] Note that the MRT results may be influenced by the model grid size due to unavoidable numerical dispersion. To understand the sensitivity of the grid size, we conducted an additional MRT calculation at M8 with 20 m grid size (the original one was 10m). The calculated average MRTs were similar: 46 days (10 m) and 50 days (20 m), and the temporal dynamics were also very similar. Thus the MRT result in this example is not significantly influenced by the grid size and the use of 10 m grid size may be justified for the acceptable computational load.

4.4. Spatial Source of Stream Water

[38] The spatial source components of the stream water were computed using T-SAS for a one year period. Figure 9

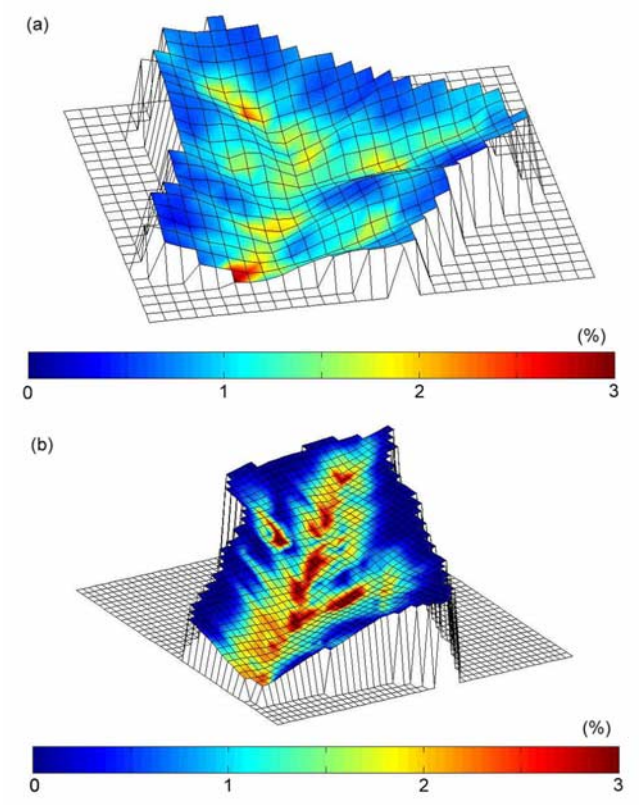

Figure 9. Spatial source distributions of total flow for 1-year simulation periods at (a) M8 and (b) WS10. For this visualization, we display the T-SAS model results over an equivalent area for each watershed and show the relative amounts contributed by different areas vary in space. The more blue colors show minimal contribution where the more red colors denote areas of maximum contribution. The scale is fractional from 0% to 3%; if we add all the values, then the total would be 100% (that is, 100% of the total flow recorded over the 1-year period).

uses colors to display the geographic distribution of flow form different places in the watershed. If all the values (colors) in the watershed map were one color (or a value of 1.0 on the percent contribution scale in Figure 9), then the spatial source of the runoff would be identical and evenly distributed across the entire watershed. On the other hand, if the values are higher than one and are unevenly distributed, then this would indicate (as in the two model examples) that certain areas of the watershed contribute more than others to runoff at the stream outlet. Results for the both watersheds show higher values of spatial source contribution at near stream zones and hollows. WS10 shows more concentrated pattern of runoff source and the pattern indicates that areas near- and immediately downslope from the ridges contributed only small amounts to flow in the stream over the 1-year simulation. This spatial source is related to the development of stream water MRT where these poorly contributing zones represent potentially long residence zones.

[39] We plot the spatial source of pre-event and event water during 30-day periods (the same periods as Figure 7) against the distance from the stream in Figure 10. Here the "Area" bar chart shows the histograms of area distributions located at different distances from the stream. The filled square and triangular plots represent the spatial source distributions of event and pre-event water during this period from different distances away from the channel. While the geographic source distributions of event water for the both watersheds are concentrated in the near stream zones, the distributions of pre-event water differ significantly between the two watersheds. The distribution at M8 follows the

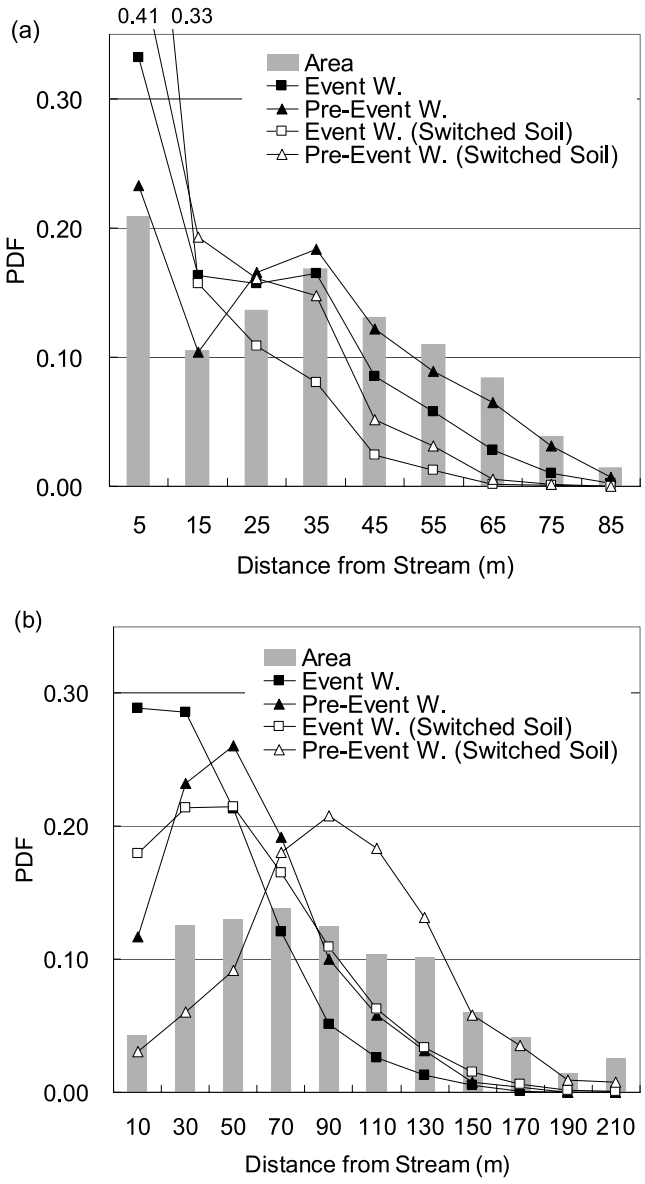

Figure 10. Geographic source distributions of event and pre-event water in PDF. The event water source is largely from the near-stream zone. Thus, the PDF for the source contribution is very different to the PDF for the area distribution (Area). For the geographic source distribution of pre-event, the M8 watershed PDF (a) follows the topography (Area) whereas the plot for WS10 shows that the proportion is higher for near-stream areas than would be expected from topography alone. When we switch the soil depths, the geographic source of pre-event water change and show more concentrated near stream sources for M8 and more distributed contributions for WS10.

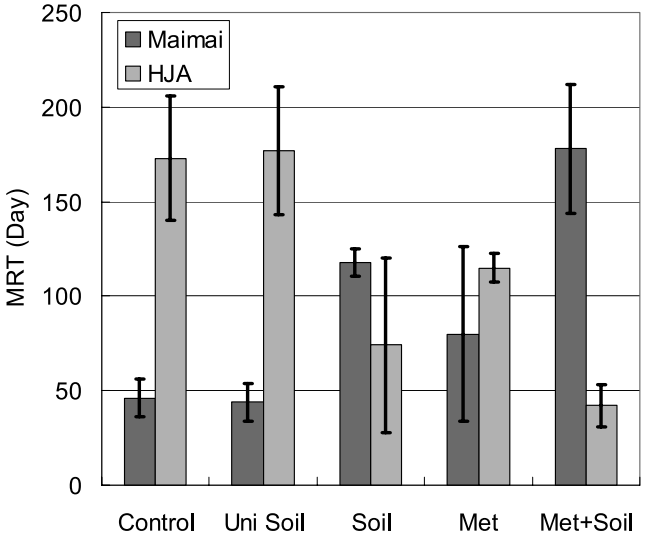

Figure 11. Virtual experiment results for MRT for M8 (dark shading) and WS10 (light shading). The bar chart shows the average MRT for a year simulation with the standard deviations computed daily over the 1-year period. "Control" represents the 1-year simulation with current conditions. "Uni Soil" is a simulation where the mean soil depth for each watershed is imposed as a uniform thickness over the entire watershed (0.7 m for M8 and 3.0 m for WS10). "Soil" represents a switching of the uniform soil thickness for each. "Met" represents a switching of the rainfall and evapotranspiration time series for each site. "Met + Soil" represent switching of both conditions for the two sites.

topography (Area) whereas the plot for WS10 shows that the proportion is higher for near stream zones than would be expected from topography alone.

[40] If we switch soil depths between M8 and WS10 (spatially uniform soil distributions with switched average soil depths) and hold all other model parameters constant (including the base case storm rainfall input), we can isolate the influence of soil depth on the spatial sources of flow. Figure 10 shows an example of this whereby the artificial increase in soil thickness at M8 decreases the direct contribution of pre-event water farther than 35 meter distance from the stream (see the unfilled dots in Figure 10). On the other hand, if we reduce the soil depth at WS10, the subsurface contributing area of pre-event water to the channel increases greatly with more catchment-wide contributions to the stream. This simple experiment shows how soil depth is a major control on the subsurface contributing area.

5. Discussion

5.1. Residence Time Damping

[41] The T-SAS approach enabled an examination of the physical meaning of MRT and how the internal dynamics of catchment response control MRT and the spatial sources of flow. In particular, we were interested in the stability of MRT and how it relates to the spatial sources of runoff. This is the first time that such linkages have been examined largely because the extreme experimental limitations of addressing this empirically and the lack of any accounting scheme in a model to reveal such behavior numerically. The model base case reproduced well the different mean residence times reported for M8 [*Stewart and McDonnell*, 1991] and WS10 [*McGuire et al.*, 2005]. More interesting is different time series dynamics of the RT through the modeled period for the two watersheds. M8 showed considerable dynamics in RT in response to rainfall events with little seasonal variability through time. Alternatively, the time series of RT at WS10 showed less dynamic response to rainfall events with higher seasonal variability. This finding suggests something fundamental about how RT varies depending upon rainfall input and storage depth damping through the watershed. Figure 11 shows the average and standard deviation of MRT for the two watersheds depending on the altered conditions. If we assume uniform soil depth but with the same soil depth average as the base case, then there is almost no difference to the "Control" simulation. This suggests that the spatial distribution of soil depth is not a major influence on the MRT at the two watersheds. On the other hand, if the average soil depths are switched between M8 and WS10 with uniform soil depths assumed in each (i.e., simply switching the measured average soil depths) this results in longer MRT at M8 than at WS10. This indicates a strong correlation between average soil depth and MRT where MRT increases with increasing soil depth. If we switch rainfall and evapotranspiration inputs between the two sites (Table 1), the effect on modeled MRT is smaller than for the soil depth switching but still results in increased M8 MRT (Figure 11). Finally, switching both soil depth and meteorological conditions for the two sites effectively reverses the observations from the control runs, implying that the difference in MRT between the two watersheds are mainly caused by the differences in the average soil depths and meteorological conditions.

5.2. On the Importance of Soil Depth for Adequate Modeling of Flow, Flow Sources, Flowpaths and Residence Times

[42] Our work shows that prediction of the headwater hydrograph with adequate modeling of sources, flowpaths and residence time of water necessitates explicit treatment of soil depth. In many ways, these findings recall the words of *Hewlett and Hibbert* [1967] who concluded from process studies that soil depth was the foremost among watershed factor affecting runoff response. While others have advocated explicit soil depth treatment in model formulations in distributed watershed models [e.g., *Saulnier et al.*, 1997; *Zhu and Mackay*, 2001] that address forest road influence [*Bowling and Lettenmaier*, 2001; *Thyer et al.*, 2004; *Whitaker et al.*, 2003; *Wigmosta and Perkins*, 2001; *Beckers and Alila*, 2004; *Storck et al.*, 1998] and watershed mixing [*Weiler and McDonnell*, 2004; *Vache and McDonnell*, 2006; *Dunn et al.*, 2007] this is the first paper, that we are aware of, that has attempted to combine flow, source, age within the model, facilitated by our new T-SAS approach.

[43] Figure 12 shows a conceptual model of our perceived relationship between MRT and spatial sources of flow based on the original diagram of *Hewlett and Troendle* [1975]. Pre-event water dominates the storm hydrograph and the event water source restricted largely to near stream zones. Soil depth and consequently soil mantle storage, strongly influences both the spatial distribution of pre-event

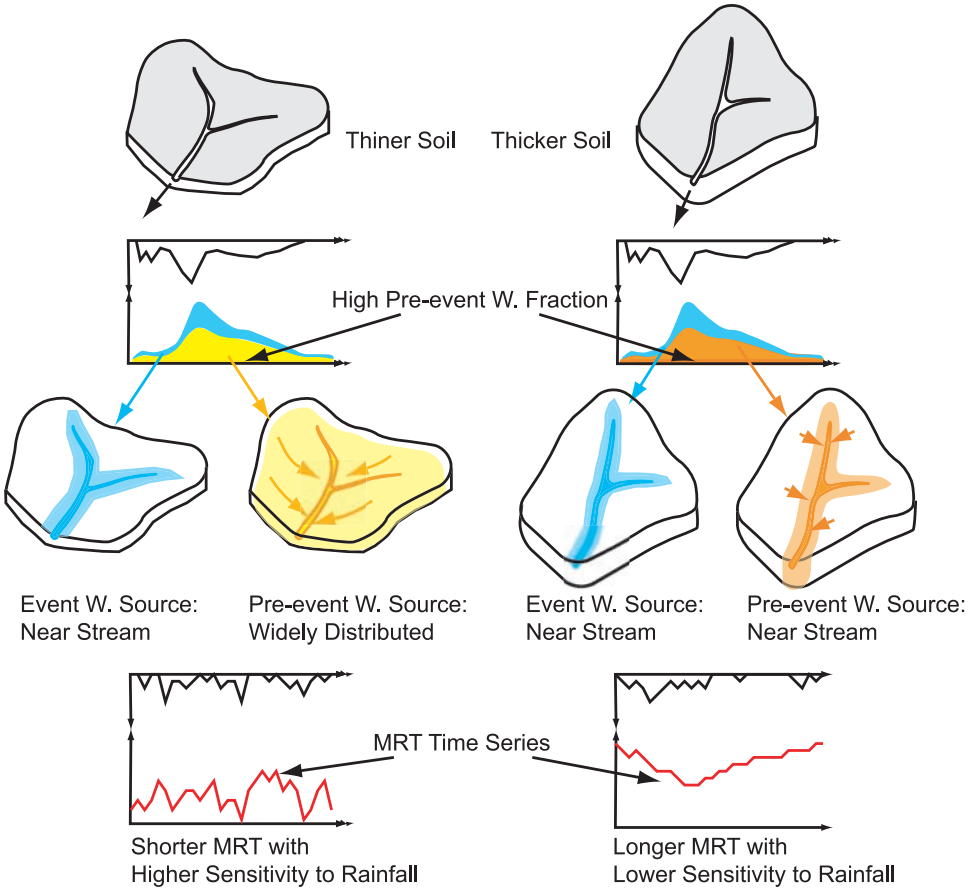

Figure 12. Conceptual model of our perceived relationship between MRT and spatial sources of flow based on the original diagram of *Hewlett and Troendle* [1975, Figure 1, page 24]. Pre-event water dominates the storm hydrograph and the event water source restricted largely to near stream zones. Soil depth and consequently soil mantle storage, strongly influences both the spatial distribution of pre-event water sources and the residence time of streamflow. Watersheds with thinner soils (and hence smaller soil mantle storage) have pre-event water sources more evenly distributed spatially within the watershed compared to the watersheds with thicker soils (and larger soil mantle storage volumes). Soil depth also affects the mean residence time and its temporal variability where watersheds with thinner soils have shorter MRT and stream MRT is sensitive to rainfall inputs.

water sources and the residence time of streamflow. Watersheds with thinner soils (and hence smaller soil mantle storage) have pre-event water sources more evenly distributed spatially within the watershed compared to the watersheds with thicker soils (and larger soil mantle storage volumes). Soil depth also affects the mean residence time and its temporal variability, as shown in Figure 11, where watersheds with thinner soils have shorter MRT and stream MRT is sensitive to rainfall inputs. While these generalized findings are consistent with recent empirical observations of MRT controls [*Stewart et al.*, 2007] they suggest that in addition to slope length and gradient [*McGuire et al.*, 2005] and soil drainage class [*Rodgers et al.*, 2005; *Soulsby et al.*, 2006] effects on MRT, soil depth may be another important factor in determining MRT (and especially RT distributions through time).

[44] Our conceptual model is also consistent with the hydrogeomorphic concept of *Sidle et al.* [2000] who noted the importance of threshold-like activation of different geomorphic positions at a steep, humid catchment in Japan. Our work extends this idea of geomorphic reservoir activation (or cryptic reservoirs activation as described by *Seibert and McDonnell* [2002]) and suggests that soil depth and its distribution in space may be an over-riding control on flow and mixing. *Sidle et al.* [2000] noted that during antecedent wetness conditions greatly influenced subsurface contributing area and its distance upslope from the stream channel. Our simulation results are consistent with these ideas where the spatial contributing area of pre-event water for both M8 and WS10 expands from the near stream zone to the upper slope areas as the watershed wets up. However, our intercomparison approach and virtual experiments point out the limitation of single-basin experimental studies for conceptual or theory development. Our simulation results for the two different watershed suggests that the subsurface expansion rate differs depending on the average soil depths; faster and farther in the shallower soil depth watershed (M8) and slower in the thicker soil depth watershed (WS10). Future work should increase the range and diversity of storage depth distributions.

[45] *Sidle et al.* [2000] also refers to the impact of soil depth on runoff generation mechanisms based on their

examination of the linkage between zero-order basins and streams. They observed that as antecedent wetness increased, zero-order basin activation began after an accumulation of shallow groundwater. Their hydrogeomorphic concept noted that the rainfall threshold to initiate the zero-order basin discharge depended on the soil depths; namely thicker soil depths require more rainfall to activate it to generate runoff. Self organization and expansion of preferential flow pathways then facilitated subsurface drainage. While our model does not explicitly simulate the detailed processes of preferential flow pathways, recent work by *Weiler and McDonnell* [2007] provide a conceptual hillslope-scale linkage between the experimental work of *Sidle et al.* [2000] and the present watershed model analysis. Such a multiscale integration approach is in development. Lastly, we should note that recent hydropedological descriptions of watershed behavior [*Lin et al.*, 2006; *McDonnell et al.*, 2007; *Pachepsky et al.*, 2008] appear very much in line with the findings presented in this paper and this explicit treatment of soil depth in particular shows an exciting pathway forward for future work that aims to rise to the Hewlett and Troendle challenge of models capture more than just flow.

6. Conclusions

[46] *Hewlett and Troendle* [1975] challenged the hydrology community over 30 years ago by arguing that accurate prediction of the headwater hydrograph implies adequate modeling of sources, flowpaths and residence times of water. To date, we have not yet been able to deconvolve the storm hydrograph into the rain parcels that fell beforehand and that express themselves at varying times in the flow regime nor are we able to apportion within the hydrograph the geographic sources of flow at different times. This paper has presented a time-space accounting scheme (T-SAS) to enable recording of the time and source components of the hydrograph. We tested T-SAS against two well known watershed benchmarks and then used it to examine fundamental questions of how the sources and age of flow at the watershed scale interact and how the time and space sources of flow are related to dominant catchment properties. Our model experiments with T-SAS suggested that the average soil depth was the first order control for the difference of MRT between the two sites. This work suggests that a catchment with thicker soil depth exhibits longer and more damped stream MRT in response to rainfall inputs. Furthermore, the spatial water sources are more concentrated to area near the stream if a catchment with thicker soil depth. These results have implications the importance of reasonable average soil depth representation and consequently soil mantle storage in a hydrologic model in order to identify spatiotemporal information of streamflow. Finally while this study focused on understanding hydrograph sources and residence time of water at shallow subsurface flow dominated watersheds, the demonstrated approach can be applied to any other watersheds with different runoff generation mechanisms. For example, a watershed with significant deep groundwater contribution, where one can investigate the impact of deep groundwater processes on the age and geographic source of streamflow. Moreover, since T-SAS can be applied to any kind of distributed rainfall-runoff models, the demonstrated approach with observed age and source information is effective to assess hydrologic model structures and their parameters.

[47] **Acknowledgments.** The first author acknowledges the funding support by JSPS Postdoctoral Fellowships for Research Abroad to conduct this study. We thank Kaoru Takara and Yasuto Tachikawa at Kyoto University for useful discussions during the development stage of the approach. We also thank many researchers who have worked at Maimai and HJA and/or these data sets: Brian McGlynn, Kevin McGuire, Kellie Vache, Markus Weiler and Jim Freer. Discussions with Luisa Hopp, Chris Graham, Holly Barnard and Cody Hale at OSU contributed to our understanding of the hydrological meaning of the simulation results. Finally, we thank to the editor and three anonymous reviewers for their useful comments.

References

Beckers, J., and Y. Alila (2004), A model of rapid preferential hillslope runoff contributions to peak flow generation in a temperate rain forest watershed, *Water Resour. Res.*, *40*, W03501, doi:10.1029/2003WR002582.

Beven, K. (2002), Towards a coherent philosophy for modeling the environment, *Proc. Math. Phys. Eng. Sci.*, *458*, 2465–2484.

Bowling, L., and D. Lettenmaier (2001), The effects of forest roads and harvest catchment hydrology in a mountainous maritime environment, in *Land-Use and Watersheds: Human Influence on Hydrology ad Geomorphology in Urban and Forest Areas*, *AGU Water and Science Application*, vol. 2, edited by M. Wigmosta and S. Burges, pp. 145–164.

Ciarapica, L., and E. Todini (2002), TOPKAPI: A model for the representation of the rainfall-runoff process at different scales, *Hydrol. Processes*, *16*, 207–229, doi:10.1002/hyp.342.

Dunn, S. M., J. J. McDonnell, and K. B. Vache (2007), Factors influencing the residence time of catchment waters: A virtual experiment approach, *Water Resour. Res.*, *43*, W06408, doi:10.1029/2006WR005393.

Fenicia, F., J. J. McDonnell, and H. H. G. Savenije (2008), Learning from model improvement: On the contribution of complementary data to process understanding, *Water Resour. Res.*, *44*, W06419, doi:10.1029/2007WR006386.

Greenland, D. (1994), The Pacific Northwest regional context of the climate of the H. J. Andrews experimental forest long-term ecological research site, *Northwest Sci.*, *69*, 81–96.

Hargreaves, G. H., and Z. A. Samani (1985), Reference crop evapotranspiration from temperature, *Appl. Eng. Agric.*, *1*, 96–99.

Harr, R. D. (1977), Water flux in soil and subsoil on a steep forested slope, *J. Hydrol.*, *33*, 37–58.

Harr, R. D., and F. M. McCorison (1979), Initial effects of clearcut logging on size and timing of peak flows in a small watershed in western Oregon, *Water Resour. Res.*, *15*(1), 90–94.

Harr, R. D., and D. W. Ranken (1972), Movement of water through forested soils in steep topography, *Coniferous Forest Biome Internal Rep. 117*, Univ. of Washington, Seattle, Wash.

Hewlett, J. D., and A. R. Hibbert (1967), Factors affecting the response of small watersheds to precipitation in humid areas, in *International Symposium on Forest Hydrology*, edited by W. E. Sopper and H. W. Lull, pp. 275–290, Pergamon, Oxford, U. K.

Hewlett, J. D., and C. A. Troendle (1975), Non-point and diffused water sources: A variable source area problem, in *Watershed Management*, pp. 21–46, Am. Soc. of Civil Eng., New York.

Iorgulescu, I., K. J. Beven, and A. Musy (2007), Flow, mixing, and displacement in using a data-based hydrochemical model to predict conservative tracer data, *Water Resour. Res.*, *43*, W03401, doi:10.1029/2005WR004019.

Kampf, S. K., and S. J. Burges (2007), A framework for classifying and comparing distributed hillslope and catchment hydrologic models, *Water Resour. Res.*, *43*, W05423, doi:10.1029/2006WR005370.

Kendall, C., J. J. McDonnell, and W. Gu (2001), A look inside "black box" hydrograph separation models: A study at the Hydrohill catchment, *Hydrol. Processes*, *15*, 1877–1902, doi: 10.1002/hyp.245.

Kirchner, J. W. (2006), Getting the right answers for the right reasons: Linking measurements, analyses, and models to advance the science of hydrology, *Water Resour. Res.*, *42*, W03S04, doi:10.1029/2005WR004362.

Leibenzon, L. S. (1947), *Flow of Natural Liquid and Gasses in Porous Medium (in Russian)*, Gostekhizdat, Moscow.

Lin, H., J. Bouma, Y. Pachepsky, A. Western, J. Thompson, R. van Genuchten, H.-J. Vogel, and A. Lilly (2006), Hydropedology: Synergistic integration of pedology and hydrology, *Water Resour. Res.*, *42*, W05301, doi:10.1029/2005WR004085.

McDonnell, J. J. (1989), The age, origin and pathway of subsurface stormflow in a steep, humid headwater catchment, Ph.D. dissertation, 270 pp., Univ. of Canterbury, Christchurch, New Zealand.

McDonnell, J. J. (1990), A rationale for old water discharge through macropores in a steep, humid catchment, *Water Resour. Res.*, *26*(11), 2821–2832.

McDonnell, J. J. (1997), Comment on "The changing spatial variability of subsurface flow across a hillside" by Ross Woods and Lindsay Rowe, *J. Hydrol. (NZ)*, *36*(1), 97–100.

McDonnell, J. J., et al. (2007), Moving beyond heterogeneity and process complexity: A new vision for watershed hydrology, *Water Resour. Res.*, *43*, W07301, doi:10.1029/2006WR005467.

McGlynn, B. L., J. J. McDonnell, and D. D. Brammer (2002), A review of the evolving perceptual model of hillslope flowpaths at the Maimai catchments, New Zealand, *J. Hydrol.*, *257*, 1–26.

McGuire, K. J. (2004), Water residence time and runoff generation in the Western Cascades of Oregon, Ph.D. dissertation, 224 pp., Oregon State Univ., Oreg.

McGuire, K. J., and J. J. McDonnell (2006), A review and evaluation of catchment transit time modeling, *J. Hydrol.*, *330*, 543–563.

McGuire, K. J., J. J. McDonnell, M. Weiler, C. Kendall, B. L. McGlynn, J. M. Welker, and J. Seibert (2005), The role of topography on catchment-scale water residence time, *Water Resour. Res.*, *41*, W05002, doi:10.1029/2004WR003657.

McGuire, K. J., M. Weiler, and J. J. McDonnell (2007), Integrating tracer experiments with modeling to assess runoff processes and water transit times, *Adv. Water Resour.*, *30*, 824–837.

McKie, D. A. (1978), A study of soil variability within the Blackball Hill Soils, Reefton, New Zealand, M.Ag.Sc. Thesis, 180 pp., Univ. of Canterbury, Christchurch, New Zealand.

Mosley, M. P. (1979), Streamflow generation in a forested watershed, New Zealand, *Water Resour. Res.*, *15*(4), 795–806.

Pachepsky, Y., D. Gimenez, A. Lilly, and A. Nemes (2008), Promises of hydropedology. Perspectives in Agriculture, *Vet. Sci., Nutr. Nat. Resour.*, *3*(040), 1–19.

Page, T., K. J. Beven, J. Freer, and C. Neal (2007), Modelling the chloride signal at Plynlimon, Wales, using a modified dynamic TOPMODEL incorporating conservative chemical mixing (with uncertainty), *Hydrol. Processes*, *21*, 292–307, doi: 10.1002/hyp.6186.

Pearce, A. J., M. K. Stewart, and M. G. Sklash (1986), Storm runoff generation in humid headwater catchments: 1. Where does the water come from?, *Water Resour. Res.*, *22*(8), 1263–1272.

Rodgers, P., C. Soulsby, and S. Waldron (2005), Stable isotope tracers as diagnostic tools in upscaling flow path understanding and residence time estimates in a mountainous mesoscale catchment, *Hydrol. Processes*, *19*, 2291–2307, doi:10.1002/hyp.5677.

Rowe, L. K., and A. J. Pearce (1994), Hydology and related changes after harvesting native forest catchments and establishing pinus radiata plantations: Part 2. The native forest water balance and changes in streamflow after harvesting, *Hydrol. Processes*, *8*(4), 281–297, doi:10.1002/hyp.3360080402.

Saulnier, G., K. Beven, and C. Obled (1997), Including spatially variable effective soil depths in TOPMODEL, *J. Hydrol.*, *202*, 158–172.

Sayama, T., Y. Tachikawa, K. Takara, and Y. Ichikawa (2006), Distributed rainfall-runoff analysis in a flow regulated basin having multiple multipurpose dams, in *Predictions in Ungauged Basins: Promise and Progress*, *IAHS Publ.*, vol. 303, pp. 371–381.

Seibert, J., and J. J. McDonnell (2002), On the dialog between experimentalist and modeler in catchment hydrology: Use of soft data for multicriteria model calibration, *Water Resour. Res.*, *38*(11), 1241, doi:10.1029/2001WR000978.

Sidle, R., Y. Tsuboyama, S. Noguchi, I. Hosoda, M. Fujieda, and T. Shimizu (2000), Stormflow generation in steep forested headwaters: A linked hydrogeomorphic paradigm, *Hydrol. Processes*, *14*, 369–385.

Sklash, M. G., M. K. Stewart, and A. J. Pearce (1986), Storm runoff generation in humid headwater catchments: 2. A case study of hillslope and low-order stream response, *Water Resour. Res.*, *22*(8), 1273–1282.

Sollins, P., and F. M. McCorison (1981), Nitrogen and carbon solution chemistry of an old growth coniferous forest watershed before and after cutting, *Water Resour. Res.*, *17*(5), 1409–1418.

Son, K., and M. Sivapalan (2007), Improving model structure and reducing parameter uncertainty in conceptual water balance models through the use of auxiliary data, *Water Resour. Res.*, *43*, W01415, doi:10.1029/2006WR005032.

Soulsby, C., D. Tetzaff, P. Rodgers, S. Dunn, and S. Waldron (2006), Runoff processes, stream water residence time and controlling landscape charactersitics in a mesoscale catchment: An initial evaluation, *J. Hydrol.*, *325*, 197–221.

Stewart, M. K., and J. J. McDonnell (1991), Modeling base flow soil water residence times from deuterium concentrations, *Water Resour. Res.*, *27*(10), 2681–2693.

Stewart, M. K., J. Mehlhorn, and S. Elliott (2007), Hydrometric and natural tracer (oxygen-18, silica, tritium and sulphur hexafluoride) evidence for a dominant groundwater contribution to Pukemanga Stream, *Hydrol. Processes*, *21*, 3340–3356, doi: 10.1002/hyp.6557.

Storck, P., L. Bowling, P. Wetherbee, and D. Lettenmaier (1998), Application of GIS-based distributed hydrology model for prediction of forest harvest effects on peak streamflows in the Pacific Northwest, *Hydrol. Processes*, *12*, 889–904.

Swanson, F. J., and M. E. James (1975), Geology and geomorphology of the H. J. Andrews experimental forest, *USDA Forest Service Res. Pap., PNW-188*, Pacific Northwest Forest and Range Experiment Station Forest Service, Oreg.

Tachikawa, Y., G. Nagatani, and K. Takara (2004), Development of stage-discharge relationship equation incorporating saturated-unsaturated flow mechanism (in Japanese), *Ann. Hydraul. Eng., Jpn. Soc. Civil Engrs.*, *48*, 7–12.

Tachikawa, Y., R. K. Shrestha, and T. Sayama (2006), Flood prediction in Japan and the need for guidelines for flood runoff modelling in predictions in ungauged basins: International perspectives on the state of the art and pathways forward, *IAHS Publ.*, *301*, 78–86.

Takasao, T., and M. Shiiba (1988), Incorporation of the effect of concentration of flow into the kinematic wave equations and its applications to runoff system lumping, *J. Hydrol.*, *102*, 301–322.

Thyer, M., J. Beckers, D. Spittlehouse, Y. Alila, and R. Winkler (2004), Diagnosing a distributed hydrologic model for two high-elevation forested catchments based on detailed stand- and basin-scale data, *Water Resour. Res.*, *40*, W01103, doi:10.1029/2003WR002414.

Uhlenbrook, S., and C. Leibundgut (2002), Process-oriented catchment modelling and multiple-response validation, *Hydrol. Processes*, *16*, 423–440, doi:10.1002/hyp.330.

Uhlenbrook, S., R. Stefan, and N. Tilch (2004), Hydrological process representation at the meso-scale: The potential of a distributed, conceptural catchment model, *J. Hydrol.*, 278–296, doi:10.1016/j.jhydrol.2003.12.038.

Vache, K. B., and J. J. McDonnell (2006), A process-based rejectionist framework for evaluating catchment runoff model structure, *Water Resour. Res.*, *42*, W02409, doi:10.1029/2005WR004247.

Weiler, M., and J. J. McDonnell (2004), Virtual experiments: A new approach for improving process conceptualization in hillslope hydrology, *J. Hydrol.*, *285*, 3–18, doi:10.1016/S0022-1694(03)00271-3.

Weiler, M., and J. J. McDonnell (2007), Conceptualizing lateral preferential flow and flow networks and simulating the effects on gauged and ungauged hillslopes, *Water Resour. Res.*, *43*, W03403, doi:10.1029/2006WR004867.

Whitaker, A., Y. Alila, J. Beckers, and D. Toews (2003), Application of the distributed hydrology soil vegetation model to Redfish Creek, British Columbia: Model evaluation using internal catchment data, *Hydrol. Processes*, *17*, 199–224, doi:10.1002/hyp.1119.

Wigmosta, M. S., and W. A. Perkins (2001), Simulating the effects of forest roads on watershed hydrology, in *Land Use and Watersheds: Human Influence on Hydrology and Geomorphology in Urban and Forest Areas*, *AGU Water Science and Application*, vol. 2, edited by M. Wigmosta and S. Burges, pp. 127–143.

Wigmosta, M. S., L. W. Vail, and D. P. Lettenmaier (1994), A distributed hydrology-vegetation model for complex terrain, *Water Resour. Res.*, *30*(6), 1665–1679.

Wissmeier, L., and S. Uhlenbrook (2007), Distributed, high-resolution modelling of 18O signals in a meso-scale catchment, *J. Hydrol.*, *332*, 497–510, doi:10.1016/j.jhydrol.2006.08.003.

Woods, R., and L. Rowe (1996), The changing spatial variability of subsurface flow accross a hillside, *J. Hydrol. (NZ)*, *35*(1), 49–84.

Zhu, A. X., and D. S. Mackay (2001), Effects of spatial detail of soil information on watershed modeling, *J. Hydrol.*, *248*, 54–77.

J. J. McDonnell and T. Sayama, Department of Forest Engineering, Resources and Management, Oregon State University, 17 Peavy Hall, Corvallis, OR 97331, USA. (sayama@flood.dpri.kyoto-u.ac.jp)